Turk J Pharm Sci 2025;22(4):246-260
DOI: 10.4274/tjps.galenos.2025.36559

ORIGINAL ARTICLE

Nanobubble-Enhanced Oral Delivery of Bortezomib: Optimizing Preparation and Characterization through Design of Experiment (DOE)

Narendra KUNDAVARAPU[1]*, Kannadasan MAHALINGAM[1], Kiran Kumar YADA[2]

[1]Motherhood University Faculty of Pharmaceutical Sciences, Department of Pharmaceutics, Uttarakhand, India
[2]Gate Institute of Pharmaceutical Sciences, Telangana, India

ABSTRACT

Objectives: Bortezomib (BTZ) functions as an androgen receptor signalling inhibitor, is used for the treatment of prostate cancer, and has been sanctioned by the United States Food and Drug Administration. The medicinal applications of BTZ are impeded by low solubility, first-pass metabolism, and restricted bioavailability. This study aimed to develop and enhance polylactic acid-co-glycolic acid (PLGA) nanobubbles (NBs) as a sustained-release mechanism for BTZ, thereby augmenting stability and bioavailability.

Materials and Methods: Seventeen experimental runs were conducted to optimize drug-PLGA NBs using a three-factor, three-level Box-Behnken Design. The improved formulation comprised 30 mg of medication, 250 mg of PLGA, and 2.0% *w/v* polyvinyl alcohol as a stabilizing agent.

Results: The NBs exhibited a particle size of 186.9±13.9 nm, a polydispersity index of 0.146±0.042, and a zeta potential of -21.4±2.28 mV, along with an entrapment efficiency of 66.12±1.48%. Fourier transform infrared spectroscopy, differential scanning calorimetry, and X-ray diffraction analysis verified the absence of drug-polymer interactions, whereas scanning electron microscopy demonstrated uniform spherical nanoparticles. *In vitro* experiments demonstrated superior drug release, and stability assessments indicated no major alterations after one month. Pharmacokinetic studies in rats demonstrated an elevated C_{max} (1.69) and area under the curve from time 0 to t (1.63), signifying enhanced sustained release and absorption. The results underscore the capability of BTZ-loaded PLGA NBs to augment drug kinetics and bioavailability, hence facilitating targeted distribution and enhanced therapeutic efficacy.

Conclusion: This investigation offered significant insights into the factors influencing oral absorption in NB formulations, which can guide future methods for oral medication development. BTZ-loaded PLGA nanobubbles showed promising results by enhancing oral absorption and improving pharmacokinetics in the study, which points to their potential use in sustained-release drug delivery. These findings offer a stepping stone toward nanomedicine via the oral route in future drug development.

Keywords: Acoustics, Box-Behnken design, BTZ, design of experiment, nanobubbles, PLGA

INTRODUCTION

B lymphocytes are a type of white blood cell that is impacted by multiple myeloma (MM), a cancerous condition. It is identified by the aberrant proliferation of a single bone marrow-derived plasma cell that produces monoclonal immunoglobulins.[1] MM is the second most common haematological malignancy, accounting for 1% of all cancers and 13% of haematological cancers.[2,3] One promising approach for treating MM is targeting the ubiquitin proteasome system (UPS).[4] The UPS is responsible for degrading defective proteins by recognizing poly-ubiquitin chains attached to them. Inhibiting proteasome activity leads to the accumulation of cells, triggering apoptosis or programmed cell death. Proteasome inhibitors have shown

***Correspondence:** narendranaidukundavarapu@gmail.com, **ORCID-ID:** orcid.org/0009-0005-8557-9676
Received: 15.07.2024 , **Accepted:** 08.06.2025 **Publication Date:** 05.09.2025

Cite this article as: KUNDAVARAPU N, MAHALINGAM K, YADA KK. Nanobubble-enhanced oral delivery of bortezomib: optimizing preparation and characterization through design of experiment (DOE). Turk J Pharm Sci. 2025;22(4):246-260

potential as antitumor agents and can also inhibit angiogenesis (anti-angiogenic properties) by blocking the UPS. Bortezomib (BTZ) (Velcade®), an approved drug by the Food and Drug Administration, is commonly used as a first-line treatment for MM and mantle cell lymphoma.[5] By acting as a proteasome inhibitor, BTZ binds reversibly to the chymotrypsin-like subunit of the 26S proteasome. This mechanism inhibits the proteasome, ultimately halting the breakdown of various pro-apoptotic factors.[6] BTZ is offered in intravenous (IV) and subcutaneous formulations. Mannitol, at a concentration of 10 mg per gram of BTZ, is used to improve solubility upon reconstitution (Velcade®). The sugar molecule helps in BTZ dissolution by forming a BTZ trimer and boronate ester, through covalent binding with the boronic acid moiety of BTZ. This ester prevents trimer formation, which could reduce water solubility. Moreover, mannitol, a highly water-soluble polyol, lowers the pKa of BTZ by three units, further increasing water solubility.[7]

The main issue with the current formulation of BTZ, which utilizes mannitol for solubility enhancement, lies in its lack of suitability for long-term drug delivery. Mannitol aids in BTZ dissolution and increases water solubility. However, its use as a cosolvent in the formulation may pose challenges for sustained drug release over an extended period. Mannitol's rapid dissolution and clearance from the body may lead to a shorter duration of therapeutic effect, necessitating frequent administration to maintain therapeutic levels of BTZ. Therefore, alternative formulations or delivery strategies that ensure sustained release and prolonged therapeutic efficacy may be required for long-term use of BTZ.

Despite the favourable clinical results, the use of BTZ has been limited because it depends heavily on proteasome function, leading to toxicity. Moreover, the medication is linked to various adverse reactions.[5,8] Additionally, BTZ is faced with pharmaceutical challenges due to its low water solubility (pKa value of 13) and a brief half-life in the bloodstream.[5] The combination of toxicity and unfavourable pharmaceutical characteristics creates substantial barriers to its use in clinical settings. As a result, there is an urgent need for a specialized formulation of BTZ. The various physicochemical and pharmacokinetic properties of BTZ are listed in Supplementary Table 1.

Therefore, a strategy that reduces the pharmacokinetic variations between the fed and fasting states must be developed. Strategies such as liposomal formulations, polymeric particles, and self-microemulsifying drug delivery systems are designed to improve the bioavailability of the drug.[9-11] *In vivo* performance, scalability issues, and the need for costly and specialised branded excipients are the obstacles with the reported approaches. Beyond enhancing solubility, an approach that offers the potential to target drug molecules specifically to diseased tissues while reducing their concentration in normal tissues is essential. Such a targeted delivery system will improve stability in bodily fluids, optimize concentration and release kinetics in the bloodstream, and enhance pharmacokinetic and pharmacodynamic properties. All these factors collectively contribute to heightened efficacy and reduced side effects. One example is the Smart delivery system, which is currently focused on cancer treatment.

At the forefront of these innovative delivery systems are smart delivery systems, which have garnered significant attention and focus, particularly in the realm of cancer treatment. By leveraging advanced technologies and principles, delivery systems that are precisely targeted and regulated represent a state-of-the-art method for administering medication aimed at navigating drugs to their intended targets within the body. Through the integration of sophisticated mechanisms, these systems hold the potential to revolutionize cancer therapy by maximizing efficacy and minimizing the impact on healthy tissues.

A smart drug delivery system possesses the ability to react to sudden changes in its surroundings, particularly those brought on by chemical stimuli. Extensive research has been conducted on the application of pressure waves and ultrasonic (US) triggers in drug delivery systems, which are dependent on external stimuli.[12]

The potential for targeted therapy in a range of medical applications has been enhanced by the broad exploration of these external stimuli to establish precise control over medication release.

Nanobubbles (NBs), or microscopic bubbles at the nanoscale, are used in numerous fields, most notably in drug delivery systems. Their amazing stability, high internal pressure, and large surface-to-volume ratio are only a few of their outstanding physical characteristics.[13]

Drugs and other therapeutic agents can be efficiently delivered to cancer cells by using NBs as carriers. NBs can vary in size from 1 nm to 500 nm, and their dimensions can be precisely tailored to the nanoscale using amphiphilic polymers such as Pluronic or surfactants. By improving blood-brain barrier penetration, NBs provide opportunities for focused drug delivery in neurological diseases, including Alzheimer's and Parkinson's. They also show potential in cardiovascular illnesses for precise thrombolytic therapy, enhancing clot breakup with fewer side effects. Research has been done on both polymeric and lipidic NBs; however, the instability of lipid-based NBs leads to breakdown and a shorter circulation period. Poly (lactic-co-glycolic acid), or PLGA, is a special kind of nano/micro biomaterial that can be used for diverse applications such as targeted medication delivery, molecular diagnostics, tissue engineering, and gene transfer.[14] Its high stability, biodegradability, and ease of chemical modification are the favourable characteristics of the PLGA.[15]

To the best of our knowledge and based on available literature, there are no prior studies documenting the utilization of PLGA NBs for delivering BTZ to cancer cells. This study aimed to develop and enhance polylactic acid-co-glycolic acid (PLGA) NBs as a sustained-release mechanism for BTZ, thereby augmenting stability and bioavailability. The research involves the preparation of BTZ-containing NBs using PLGA, followed by comprehensive *in vitro* characterization, including analysis

of particle size (PS), size distribution, zeta potential (ZP), morphology, release kinetics, and subsequent *in vivo* evaluation.

MATERIALS AND METHODS

The pure drug BTZ was acquired from Dr. Reddy's Ltd., Hyderabad, India. Sigma Aldrich, USA, supplied Poly (D, L-lactide-co-glycolide) 50:50 with an intrinsic viscosity of 0.22 dL/g and a molecular weight of 25,000. Polyvinyl alcohol (PVA; Mw 30,000-70,000) was purchased from Sigma Aldrich (St. Louis, MO, USA). Borviz 2 injection was purchased from Intas Pharmaceuticals Ltd., Ahmedabad, India. Antipyrine was procured as a sample from M/s Yarrow Chemicals Pvt., Ltd., Hyderabad. Isopropanol and dichloromethane (DCM) were acquired from S.D. Fine Chemicals, Hyderabad. We purchased acetonitrile from Qualigens, India. The cells were purchased from NCS Pune, Maharashtra, India. All the media components were purchased from Gibco, USA, and Invitrogen, USA.

Analytical method development using reverse-phase high-performance liquid chromatography

Chromatographic analysis of BTZ was executed using a Shimadzu Prominence model LC-20 AD, equipped with an ultraviolet detector set at 230 nm. A reverse phase Luna C-18 column (150 mm × 4.6 mm *i.d.*, 5.0 µm PS and 100 Å pore size) maintained at 40.0±0.1 ˚C was employed. The mobile phase is composed of a mixture of acetonitrile and ammonium phosphate (buffer pH 4 adjusted with acetic acid) (60:40 *v/v*). The mixture was sonicated for 45 minutes for degassing purposes and then filtered through a 0.45 µm pore diameter Whatman filter paper. The flow rate was adjusted to 1.0 mL/min. A standard stock solution of the drug at a concentration of 1000 µg/mL was prepared, followed by the creation of various working standard solutions ranging from 0.5 to 100 µg/mL through serial dilutions. A stock solution (1000 µg/mL) of Antipyrine as IS (internal standard), after appropriate dilution, was included in the experiment. Retention time of drug and internal standard was 4 minutes and 6.8 minutes, respectively.[10]

BTZ-NBs formulation development and optimization

BTZ-loaded PLGA NBs were synthesized using solvent evaporation with ultrasound assistance following a reported method with slight modifications. Initially, a homogeneous solution was formed by dissolving PLGA (200 mg) in a water-immiscible solvent, DCM. The drug BTZ was then added to create a dispersion, which underwent sonication for five minutes at 45% amplitude, in an ice bath using a Digital Sonifier S-250D (Branson US, Danbury, USA). Next, the drug dispersion was combined with 25 mL of chilled 2.0% PVA solution and homogenized at 13222 rpm for 10 minutes using a high-speed homogenizer. The formulation was then subjected to sonication using a US probe at 30 W for 3 minutes. A 2.5% *v/v* isopropanol solution (25 mL) was added to the emulsion and mechanically stirred for 5 hours to remove the DCM. Subsequently, the resultant product was centrifuged at 8000 rpm for five minutes. The product was washed with distilled water after discarding the supernatant. This centrifugation and washing process was repeated three times. The NBs were freeze-dried for 36 h without exposure to light using a LYPH LOCK 4.5 (Labconco Corporation, Kansas City). Later, C3F8 gas (perfluoropropane) was added to the lyophilization chamber through a vial connector at a flow level of 50 mL/min for 1 minute. After this, the screw vials were tightly sealed for further analysis.[16] BTZ-loaded PLGA NB optimization was achieved by implementing a three-factor, three-level BBD. A total of 17 experimental runs were conducted, including three replicated centre points.[17]

The three independent variables were the amount of PVA *(w/v)*, homogenization speed (rpm), and homogenization time, each at three levels of variation: low (-1), middle (0), and high (1). The response (three dependent variables) were PS (Y1), polydispersity index (PdI) (Y2), and encapsulation efficiency (% EE) (Y3); Table 1 lists their respective ranges. Utilizing response surface charts and contour (2D) plots, the response surface search was carried out with Design Expert® (Version 12.0.3.0, Stat-Ease Inc., Minneapolis, MN).

Characterization and evaluation

Measurements of PS, PdI, and ZP

A Zetasizer (Malvern Instruments, UK) was used with DLS theory (dynamic light scattering) to calculate the PS, PdI, and ZP of BTZ NBs after tenfold dilution of the sample with double-distilled water.[18]

Percentage entrapment efficiency (% EE)

The % EE of the drug in the NBs can influence the therapeutic efficacy, stability, and release kinetics of the loaded compounds within the NBs. DCM was used to dissolve a particular quantity of NBs containing the loaded drug (BTZ) NBs. The complex was dissolved by subjecting the solution to sonication for 10 minutes. The resultant solution was then suitably diluted and assessed using the above-mentioned HPLC method.

The following equation was used to calculate the same:

$$\text{Entrapment efficiency \%} = \frac{\text{(total amount of the drug-free drug)}}{\text{(amount of drug)}} \times 100$$

Table 1. Factors influencing the experiment's design

		Levels		
	Independent variables	**Low (-1)**	**Medium (0)**	**High (+1)**
A	Amount of PVA (% *w/v*)	1.0	1.5	2.0
B	Homogenization speed (rpm)	10000	12500	15000
C	Homogenization time (mins)	5	10	15
	Dependent variables	**Restrictions**		
Y1	Particle size (nm)	Minimize		
Y2	Polydispersity index	Minimize		
Y3	EE (%)	Maximum		

PVA: Polyvinyl alcohol, EE: Encapsulation efficiency

Morphology using scanning electron microscopy (SEM)

Using a Quanta FESEM 250, the structure of the NBs and the drug was captured. Before testing, the sample was mounted on an aluminium pin stub after being mounted with double-sided carbon tape and Au-sputter coated utilizing an ion sputter. The specimen was then analysed at an operating distance of 10 millimetres, with an acceleration current of 30 kV and a magnification of 500-10,000 times.[19]

Fourier-transform infrared (FTIR) spectroscopy

The spectrum of FTIR was obtained using a Perkin-Elmer spectrometer (Model 1600; USA). The pure drug, PLGA, physical mixture (PM), and the optimized drug-loaded NBs were all analysed at wave numbers 4000-450 cm-1 with a resolution of 1.0 cm-1.[20]

Differential scanning calorimetric study and X-ray diffraction pattern (XRD)

DSC (DSC-60, Shimadzu Corp., Japan) was employed to ascertain the drug's physical structure and the potential for chemical interactions with the excipients. Samples of 3-5 mg (pure drug, blank NBs, PLGA, optimized drug-loaded NBs, and NBs stored for three months) were subjected to heating (50-400 °C, 5 °C/min) in folded aluminum pans in a nitrogen environment before being subjected to DSC analysis, following calibration using Indium and Lead standards. The melting point (MP) and the enthalpy of fusion were computed automatically. The X-ray diffraction patterns of the pure drug, the PM, and the optimized formulations were obtained using a Philips X-ray diffractometer (PW-1710) operated with a graphite monochromator and Ni-filtered Cu Kα radiation (at 100 mV and 40 kV). The samples were scanned between 2° and 60° 2 theta (θ) angle with an average step size of 0.045° and a duration per step of 0.5 seconds.[21]

Drug release

The release studies of pure drug and optimized drug-loaded PLGA NBs were carried out using *in vitro* experiments with a shake flask equipped with a dialysis bag. Following encapsulation in dialysis membranes, the specimens were transferred into a conical flask containing phosphate buffer (pH 7.4), maintained at 37 °C, and subjected to constant rotation at 100 rpm. One mL of sample was removed from the outer solution and replaced with brand-new PBS at pH 7.4 at predefined intervals. These aliquots were filtered and analysed using the HPLC method at 230 nm to measure drug release. Three duplicates of the experiment were carried out.[22]

Stability studies

The optimized formulation's stability was evaluated by storing it at three temperatures (4 °C, 25 °C, and 40 °C) at 75% relative humidity. Regular intervals were set to measure PS, PdI, and EE% % changes in the samples.[23]

Pharmacokinetic studies (PKs)

Male Wistar rats with an approximate weight of 200±20 g and an age of 4-5 weeks were procured from the National Institute of Nutrition situated in Telangana, India. The animal protocol was designed and approved by the Institutional Animal Ethics Committee of Teegala Ram Reddy College of Pharmacy (approval number: 1447/PO/Re/S/11/CPCSEA-97/A, dated: 17.02.2024). For about a week, animals were exposed to natural light/dark settings, acclimating to a relative humidity of 40–60% and a temperature of 20 °C±2 °C. Then they were split into three groups of six animals randomly. An optimized drug-loaded NB (0.2 mg/kg BW) and the pure drug (dispersed in 0.5% *w/v* carboxymethyl cellulose) were administered by the oral route, while the reference (marketed product) was given by the IV route. The animal blood was obtained from the retroorbital plexus (300 µL) and then transferred into sterile test tubes with EDTA at specific intervals (0.25, 0.5, 1, 2, 4, 6, 12, 24, 48, and 72 h). Blood samples were centrifuged at 7500 rpm for ten minutes using an Eppendorf centrifuge. The resulting plasma was further analysed using HPLC.[10]

Using the protein precipitation method, the drug was recovered from plasma samples. By adding 250 µL of acetonitrile to 50 µL of rat plasma and vortexing the mixture, the drug was effectively extracted from the plasma. After centrifuging the supernatant for 12 minutes at 8000 rpm, chromatography was used to analyze it at a wavelength of 230 nm. Non-compartmental analysis using WinNonlin (version 3.1; Pharsight Corporation, USA) was employed to calculate the C_{max} (maximum plasma concentration), AUC_0-72 (area under the plasma concentration vs. time curve from 0 to 72 h), T_{max} (time to reach the maximum plasma concentration), Kel (elimination rate constant), and t1/2 (half-life).

Statistical analysis

Non-compartmental analysis WinNonlin (version 3.1; Pharsight Corporation, USA) was employed to calculate all pharmacokinetic parameters. All the data were expressed as mean ± standard deviation.

RESULTS

BTZ-NBs formulation development and optimization

The study aimed to formulate BTZ NBs by integrating ultrasound technology with solvent evaporation. The drug had been mixed with PLGA that had been dissolved in DCM, sonicated, and added to a cooled 2.0% *w/v* PVA solution. After that, a 3-minute sonication at 30 W and high-speed homogenization were performed on the sample. Isopropanol solution (2.5% *v/v*) was used to extract DCM.[24,25]

BTZ PLGA NBs formulation optimization by Quality by Design emphasizing preciselyby monitoring critical quality attributes (CQAs) to achieve and maintain QTPP was carried out.[26] The current study selected PS, PdI, and EE as CQAs (Table 2). Multiple linear regression analysis (2FI) constructed polynomial models (quadratic, two-factor, and linear). The model selection used R^2, predicted R^2, adjusted R^2, and coefficient of variance (C.V.). Analysis of variance (ANOVA) assessed the impact of variables on responses.

Table 2. Box–Behnken Design and the experimental data

Factor 1	Factor 2	Factor 3	Response 1	Response 2	Response 3
A: Stabilizer concentration, %	B: Homogenization speed, rpm	C: Homogenization time, mins	PS (Y1), nm	PdI (Y2)	EE % (Y3)
1.5	15000	5	207.12	0.332	52.26
1	12500	5	302.88	0.416	70.03
2	12500	15	234.4	0.229	78.16
2	12500	5	244.12	0.262	61.9
1	12500	15	296	0.488	73.25
1.5	10000	5	302.03	0.32	71.94
2	10000	10	197.89	0.229	65.16
1.5	12500	10	182.78	0.182	66.44
2	15000	10	199.64	0.132	64.04
1.5	12500	10	209.26	0.234	66
1.5	12500	10	209.1	0.229	64.77
1.5	12500	10	204.7	0.244	64.08
1.5	15000	15	258.44	0.288	71.41
1	10000	10	256.3	0.418	76.47
1.5	12500	10	210.5	0.183	66.1
1.5	10000	15	199.2	0.36	68.36
1	15000	10	254	0.336	56.66

PS: Particle size, PdI: Polydispersity index, EE: Encapsulation efficiency

PS

A small size of NBs resulted in a significantly higher surface area-to-volume ratio, enhancing their stability, penetrability, and reactivity in targeted drug delivery 17. After 17 trials, PS ranged from 182.78 to 302.88 nm. The model's *f* value of 21.43, with a 0.03 percent chance of being noise, confirmed its "quadratic" nature and that the lack of fit is insignificant. The various perturbation plots of PS, PdI, and % EE are shown in Supplementary Figure 1. ANOVA found variables with p-values below 0.0500 that significantly impacted the response. The "lack of fit *f* value" (0.77) implied that any lack of fit was not statistically significant. There was a 56.84% chance that a "Lack of Fit F-value" of this extent would occur due to random noise, undermining the model's reliability. The contour plots (CP) and 3D response surface plots (RSP), illustrating variable influences on PS, were depicted in Figure 1. The R2, corrected R2, and anticipated R2, with values of 0.9650, 0.9200, and 0.7604, respectively, showed a model precision of 13.19, surpassing the required value of 4.

Stabilizer concentration (A), with a high negative coefficient, was the most influential factor affecting PS, as it demonstrated that alterations in this factor resulted in a corresponding change in PS. Stabilizer concentration, homogenization speed, and time, denoted by variables A, B, and C, also played a role in PS, although to a lesser extent than the other factors.

The interaction terms (BC) suggested a combined effect of these variables, and this had a significant impact on PS. the positive coefficients for quadratic terms like A2 and C2 indicate that the squared values of A and C have a nonlinear relationship with PS, potentially leading to changes in PS that are not directly proportional to changes in the variables. Model terms (A, B, C, BC, A^2, and C^2) had *p* values <0.0500, signifying their effect. The resulting regression equation was:

$PS = 217.63 - 28.79\,A - 23.80\,B - 24.46C + 1.01\,AB - 0.3550\,AC + 19.27B\,C + 25.67\,A^2) - 1.98\,AB^2 + 10.10\,C^2$

PdI

The PdI is a dimensionless metric that quantifies the broadness of the PS distribution.[17]

Typically, it falls between 0 and 1. Formulations exhibited PdIs from 0.132 to 0.488, with a model *f* value of 19.68, which indicated a significance of the proposed "quadratic" model and an insignificant lack of fit (*f* value 0.78). There was a 56.38% chance that a "Lack of Fit *f* value" of this magnitude would arise due to random noise, underscoring the model's reliability.

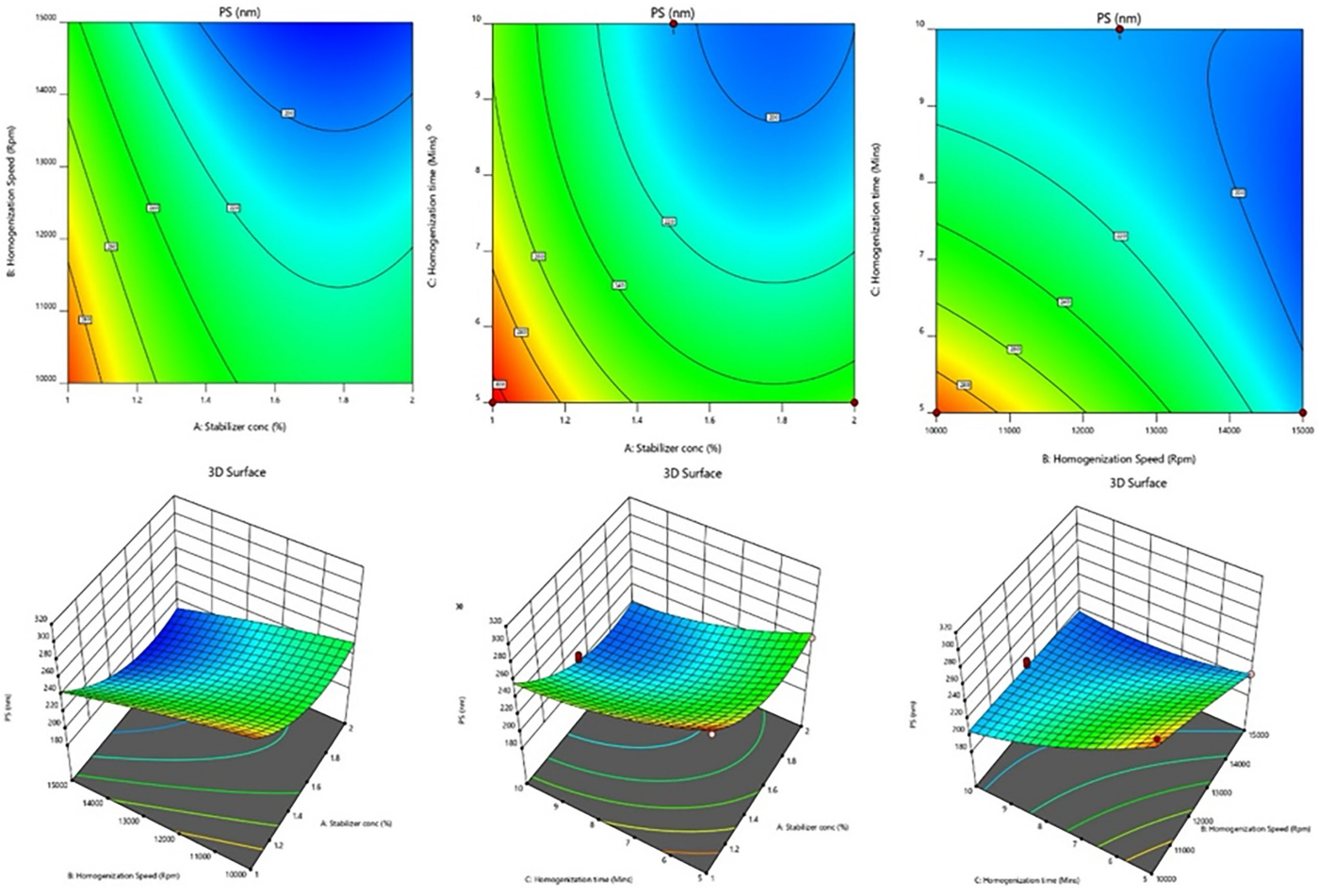

Figure 1. CPs and RSPs illustrating variable effects on PS
CPs: Contour plots, RSPs: Response surface plots, PS: Particle size

Regression coefficients (R2, adjusted R2, and anticipated R2) were 0.9620, 0.9131, and 0.7383, which showed the model's usefulness with precision exceeding the necessary value (15.5323). Model terms (A, C, A2, and C2) had *p* values <0.050, signifying a substantial impact. The resulting regression equation is:

$$PDI = 0.2348 - 0.0876\ A + 0.0194\ B - 0.0430\ C - 0.0037\ AB + 0.0131\ AC - 0.0105\ BC + 0.0440\ A^2 + 0.0203\ B^2 + 0.0226\ C^2$$

Positive coefficients signify a rise in the associated variable(s), which increases PdI, while negative coefficients indicate a decline, which reduces PdI.[27] An increase in variables A and C led to a decrease in PdI, whereas higher values of B (homogenization speed) led to higher PdI. All quadratic terms have positive coefficients, indicating that increases in the squared values of variables A, B, and C lead to increases in the PdI. The response surface and contour plots illustrating variable effects on the PdI are shown in Figure 2.

Percentage entrapment efficiency (% EE)

Impact on % EE ranged from 52.26% to 78.16%. The NB with high entrapment is always desirable, as it helps reduce the dose of the drug.[27] The model's *f* value, 63.30, with a 0.01% chance, is likely due to noise, indicating significant and negligible fit error for the suggested "quadratic" model. The F-value for lack of fit (1.41) was statistically insignificant based on pure error, with a 36.19% probability of being noise. ANOVA identified significant factors (*p* value <0.1000), which led to the removal of non-significant variables. The consequence of variables on ZP, as demonstrated by CP and RSP, is shown in Figure 3. The regression coefficients, R2, adjusted R2, and anticipated R2 were 0.9879, 0.9723, and 0.8908, respectively. The predicted R2 aligns closely with the adequate R2, differing by 0.2. The model, evidenced by an adequate precision (signal-to-noise ratio) of 31.5008, surpassing the necessary value of 4, proved helpful in exploring the design space. Figure 4 illustrates a CP and 3D SP, which showcase the influence of selected variables on % EE. An elevation in factors A and B, both related to stabilizer concentration, typically results in decreased entrapment efficiency. In contrast, the interaction terms and quadratic terms increased the percentage of EE. By comprehending the impact of these factors on entrapment, researchers can fine-tune formulations to attain desired levels of efficiency, thereby guaranteeing the effective delivery of substances in

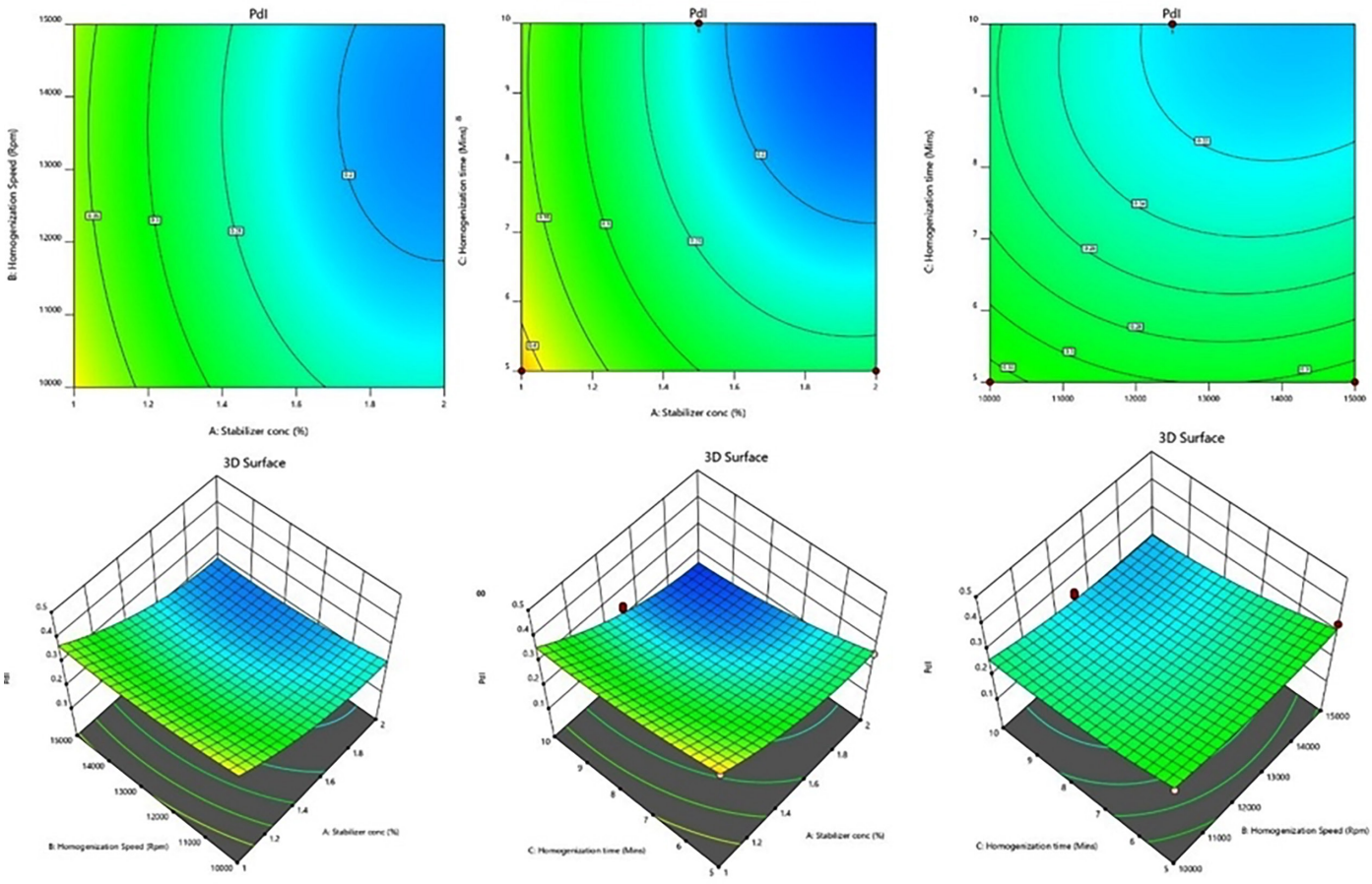

Figure 2. Graphical depiction of contour plots and response surface plots illustrating variable effects on PdI
PdI: Polydispersity index

pharmaceutical or other applications. Model terms (A, B, AB, AC, BC, A^2, B^2, and C^2) had *p* values <0.0500, signifying a significant effect. The resulting regression equation is:

$$EE\% = +64.01 - 2.51\,A - 7.54\,B + 0.7489\,C + 4.67\,AB + 1.63\,AC + 2.84\,BC + 2.47\,A^2 - 2.37\,B^2 + 0.7209\,C^2$$

Characterization and evaluation of NBs

PS, PdI, ZP, % EE, and morphology

PSs and uniformity in the formulation remained consistent, with PS of 186.9±13.9 nm and PdI of 0.146±0.042. A polydispersity value below 0.3 indicated homogeneity. The optimized formulation's ZP, indicative of colloidal particle surface properties, was -21.4±2.28 mV, with a % EE of 66.12±1.48. The PS and ZP of the optimized NBs are shown in Figure 5. NB stability heavily relies on elevated ZPs, which play a crucial role in maintaining electrostatic repulsion among particles, thus preventing their aggregation. This stability is of utmost importance as it ensures the integrity of NBs during storage and administration, ultimately enhancing their performance in drug delivery and medical imaging applications. PS and ZP were shown in Supplementary Figure 2. It was evident from the figure that the drug had a variety of PSs and a non-uniform cubic shape containing particles as small as micrometres. However, after the formation of the NB, the micronized drug particles consistently changed to spherical particles in the nanosize range.

FTIR

Figure 5 illustrates the determination of component compatibility observed for nano formulation, excipients, and plain drug infrared spectra, using a scanning range of 450 cm-1 to 4000 cm-1. Distinctive peaks in the plain medication were observed at 3446.9; 3294; 2937.68; 1747.57; 1663; 1523; 1460; 1394; 1261.49; 1193.98; 1085.96; 1022; 885.36; and 719 cm-1. There was a physical interaction between the drug and stabilizer, as evident in the stability of the apparent peaks and the absence of new peaks in both the PM and the freeze-dried formulation. The FTIR spectral data with wave number and the corresponding groups is given in Supplementary Table 2.

The stability of the evident peaks and the absence of new ones in the physical mixing and freeze-dried formulation indicate that there is physical interaction between the drug and stabilizer.[28]

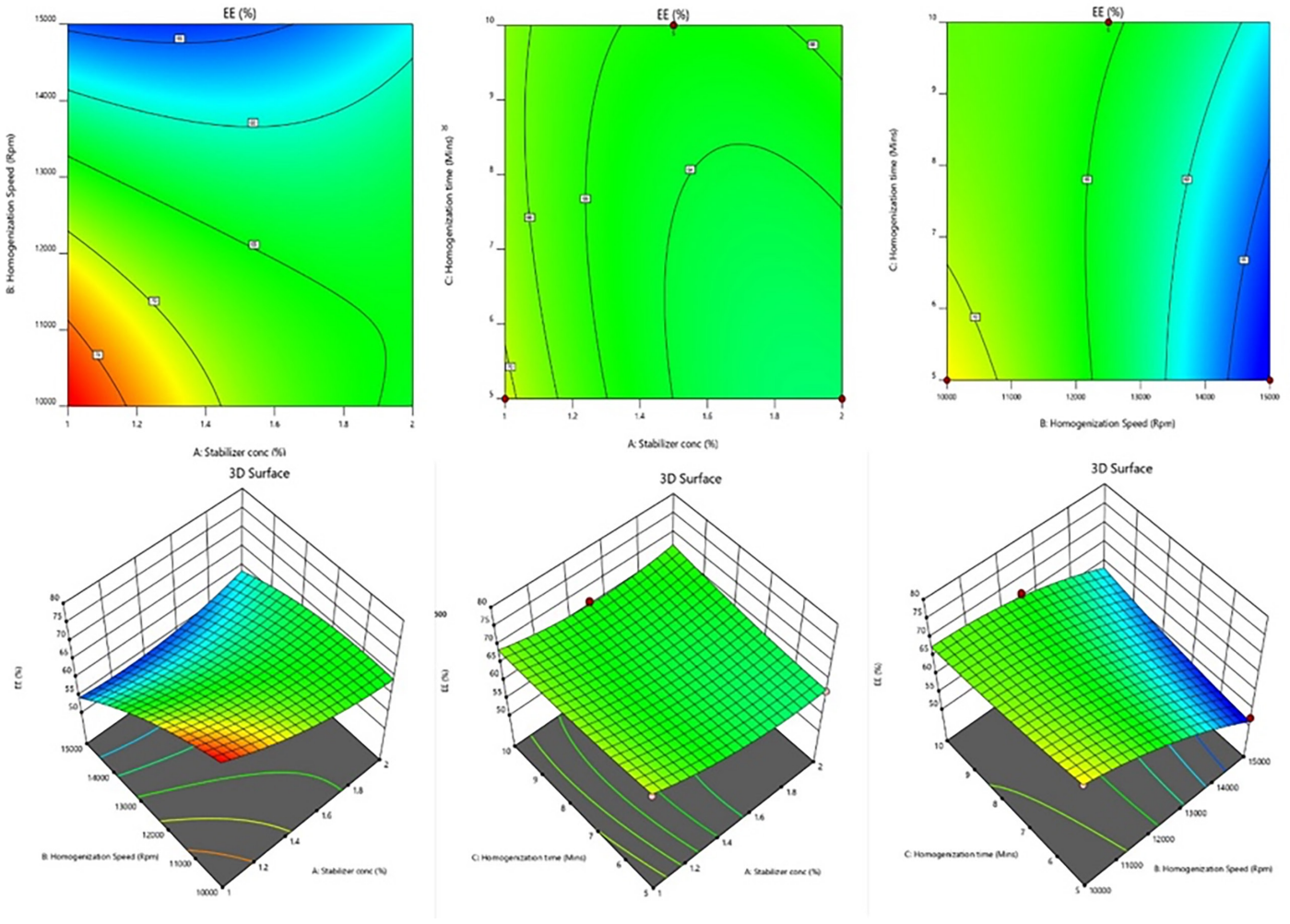

Figure 3. Graphical representation of RSPs and CPs demonstrating its consequences of variables on % EE
RSPs: Response surface plots, CP: Contour plots, EE: Encapsulation efficiency

DSC and XRD

DSC assessment was accomplished to evaluate the thermal characteristics of the drug, PLGA, and the NBs pre- and post-storage for 3 months (Figure 6). The pure drug exhibited a clear endothermic peak at 167.36 °C, signifying its MP a broad peak at 287.64 °C, and at 43.31 °C, indicating its crystalline characteristics.[28]

The thermograph of PLGA exhibited peaks at 61.8 °C and 163.17 °C. In the thermographs of the NBs, two peaks emerged at 200.52 °C and 26.18 °C, indicating the minor shifts in the MP of the drug and its confinement within the polymeric structure due to weak intermolecular interactions between the drug and the polymer.

The XRD patterns are depicted in Figure 6B. The drug has displayed firm diffraction peaks (2θ scattered angles of 12.88, 16.52, 18.07, 19.65, 20.52, 21.3, 24.06, 24.2, 24.53, and 33.530) confirming its crystalline nature.[28,29] Previous studies have also reported similar diffraction peaks for the drug under study. However, in the NBs, the characteristic diffraction peaks of BTZ vanished, suggesting the pure drug may have formed a solid-state complex at a molecular level.

Drug release

Figure 7 depicts dissolution profiles of plain drug and drug-loaded NBs with and without acoustic assistance. Drug release from NBs was significantly higher than from a simple drug suspension. Notably, ultrasound assistance increased drug release. The cumulative drug release at 8 hours was 17.24±3.32%, 40.04±4.61%, and 76.84±4.04% for plain drug, NBs without and with acoustic activation, respectively. By 48 h, over 98.14±8.47% was released from NBs with acoustic assistance and 68.02±8.26% without acoustic aid, but in the case of the pure drug, only 33.1±4.60% of the drug was released. Drug release occurred due to cavitation collapse induced by acoustic waves and disrupted NB structures, enabling rapid medication release. Acoustic waves, characterized by meticulous control and a non-invasive nature, offer accurate drug delivery and targeting abilities. These findings confirmed that ultrasound assistance plays a pivotal role in enhancing drug release from the NBs, potentially through the cavitation effect induced by ultrasound. Ultrasound stability studies indicated the transformation of the gas core, where nanodroplets turn into bubbles, known as acoustic droplet generation. Under the influence of ultrasound,

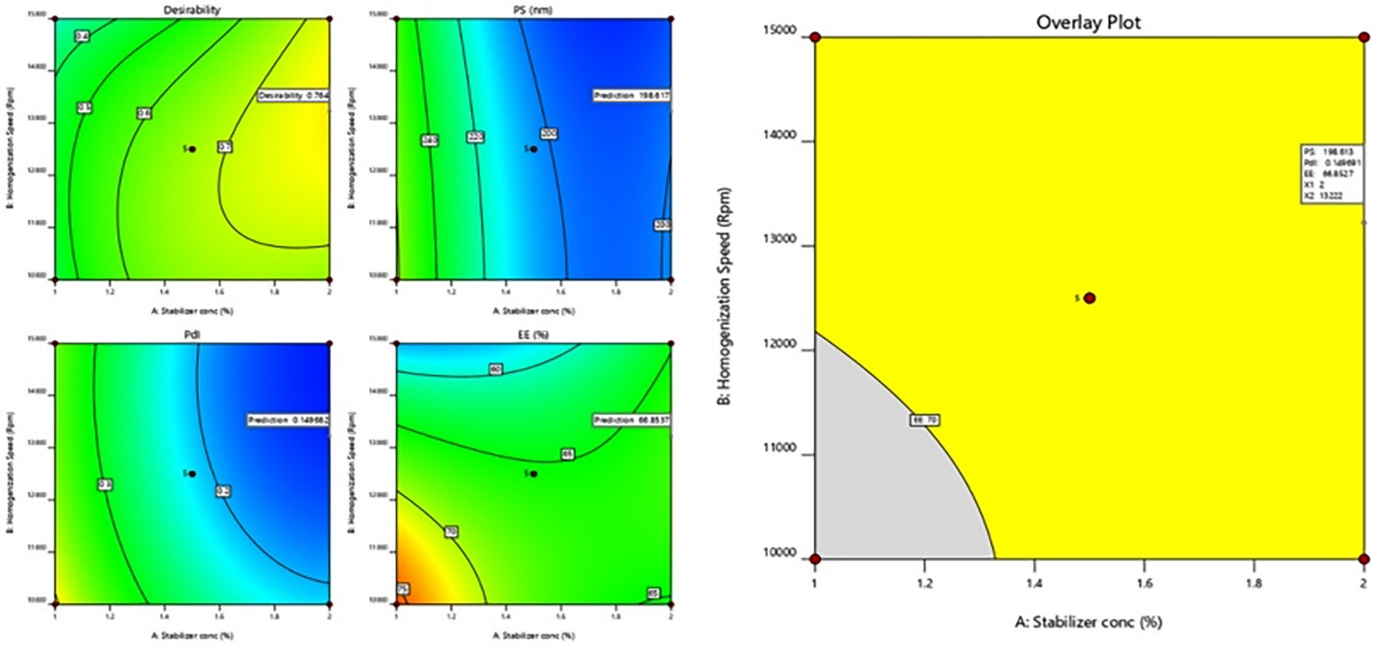

Figure 4. Graphical illustration of desirability and overlay plot (yellow area denotes the feasible region)

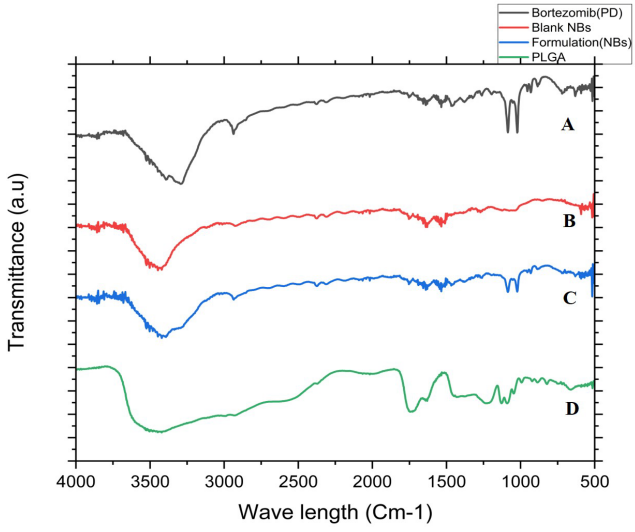

Figure 5. A) Overlay of FTIR analysis A: BTZ-PD (black line- pure drug); B: Blank NBs (red line-); C: Formulation NBs (Blue line- NB); D) PLGA (green line)

BTZ-PD: Bortezomib-pure drug, FTIR: Fourier transform infrared spectroscopy, NBs: Nanobubbles, PLGA: Poly(lactic-co-glycolic acid)

the oscillation of bubbles can trigger the shell to open, thereby aiding in the release of drugs. The study aligned with previous findings on NB stability under varying temperature conditions. The acoustic streaming flow generated by bubble oscillation regulates the movement of detached materials, which is influenced by both the radial excursion and the duration of the ultrasound pulse.[18]

Stability studies

BTZ-loaded NBs (NBs) underwent stability assessments at various storage conditions at 4 °C, at 25 °C, and at 40 °C immediately, one month, two months, and three months (Table 3). At 4 °C and 25 °C, minimal changes in drug content indicated robustness, with % EE showing slight variation, suggesting protection against degradation. However, a notable reduction in % EE occurred at elevated temperatures, where % EE was reduced to 62.41±3.90% from 65.12±2.54%, indicating structural disruption. Throughout the experiment, the PS of the formulation was less than 200 nm, and the ZP was around 29±2.29 mV, highlighting the stability and uniformity of BTZ NBs. Storage in a polyethylene pouch led to a faster drop in the number concentration compared to when stored in a glass bottle. Hydrogen bonding interactions were emphasized as critical factors in forming bulk NBs and their exceptional long-lasting stability.[17]

Pharmacokinetic studies

Figure 8 displayed the plasma concentration-time curve after drug administration in a 0.25% *w/v* sodium carboxymethyl cellulose solution and the optimized NBs, administered orally. Pharmacokinetic data in Table 4 revealed that the formulation exhibited significantly higher T_{max}, C_{max} ($p<0.001$**), AUC_0-24 ($p<0.001$**), and AUC_0-∞ ($p<0.001$**) values compared to the pure drug suspension at the prescribed dose. The bioanalytical chromatogram indicated drug retention time at 4.0 min and internal standard (Antipyrine) at 6.8 min (Supplementary Figure 3).

The optimized formulation reached a maximum level (C_{max}) 1.69 times higher, while the area under the curve (AUC_{0-t}) was 1.63 times higher than that of the free drug. *In vivo* studies revealed a progressive drug release from the NB preparation, with an

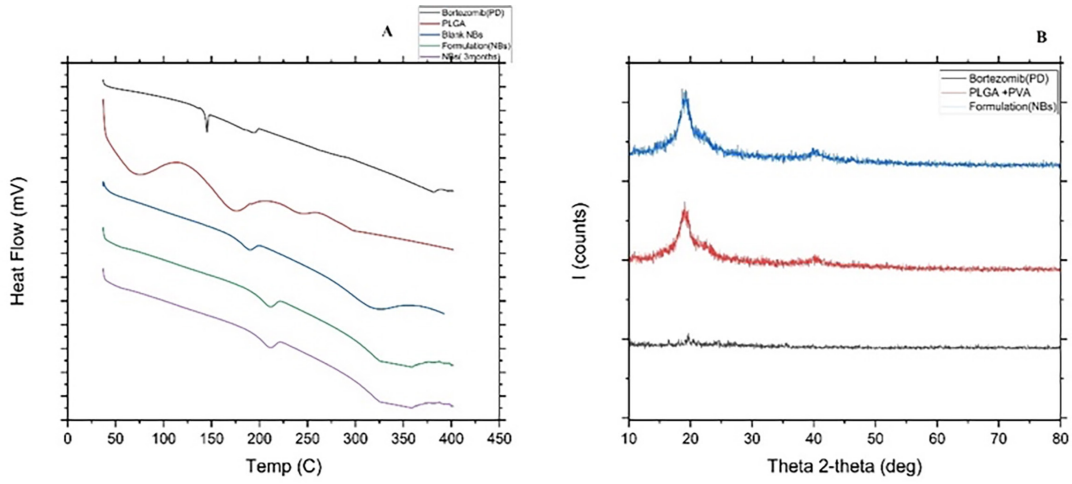

Figure 6. A) Overlay of DSC thermograms of i) BTZ-PD (black line); ii) PLGA (red line); iii) Black NBs (blue line); iv) Formulation (optimized NBs green line); v) Blanks NBs stored for 3 months (purple line); B) Overlay of XRD of i) BTZ-PD (black line); ii) PM (PLGA + PVA + drug-red line); iii) Formulation-NBs (blue line)

DSC: Differential scanning calorimetry, XRD: X-ray diffraction, BTZ-PD: Bortezomib-pure drug, PLGA: Poly(lactic-co-glycolic acid), NBs: Nanobubbles, PM: Physical mixture, PVA: Polyvinyl alcohol

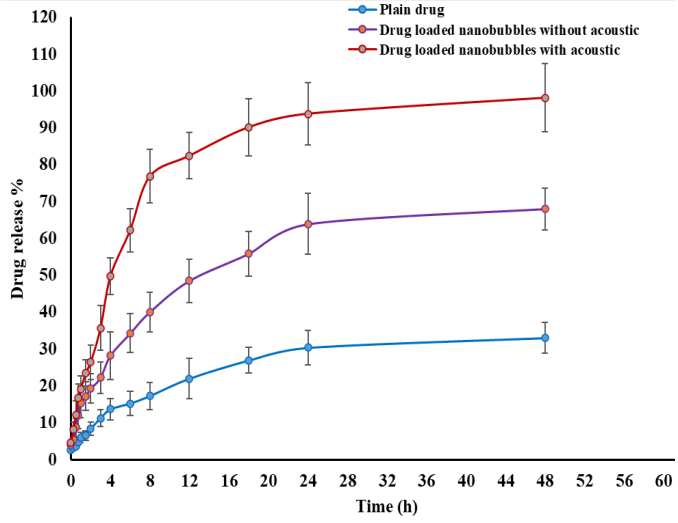

Figure 7. *In vitro* drug release of plain drug, drug-loaded NBs with and without ultrasound aid

NBs: Nanobubbles

extended half-life. The comparison of the data to the free drug shows that oral bioavailability has significantly improved. These findings suggested a notable improvement in oral bioavailability compared to the free drug. The enhanced bioavailability can be attributed to the increased drug circulation at the nanoscale and the improved penetration facilitated by the polymeric carrier system.

DISCUSSION

In this study, BTZ-loaded PLGA NBs were formulated using the solvent evaporation method, and optimization was conducted through the BBD. NBs are emerging as a formulation strategy because of their targeting ability. The process in which nanodroplets in perfluoro pentane transition from liquid to vapor upon exposure to ultrasound waves is called acoustic droplet vaporization.[24] Perfluoropentane undergoes a phase transition that turns nanodroplets into NBs with high US wave reflectivity. The echogenic qualities of perfluoropentane make it visible in ultrasonography images.[23]

The NBs were developed using PLGA polymer containing unbound carboxylic end chains, with perfluoropentane for the inner core and PLGA as the outer shell.[23] The term "ultrasound" describes mechanical vibrations or pressure waves that exhibit compressional and rarefactional pressure fluctuations and have frequencies equivalent to or higher than the human hearing threshold (20 kHz). Ultrasound effects primarily involve two mechanisms: cavitation and sonoporation. The cavitation effect plays a crucial role in reducing the size of bubbles, whereas the sonoporation effect facilitates the uptake of these reduced bubbles.[30] Hydrophobic interactions play a crucial role in bonding PLGA with the drug by forming NBs, while polyvinyl alcohol (PVA) acts as a stabilizing agent. PVA creates a protective coating around the NBs to uphold their stability. Due to its biocompatibility and biodegradability properties.

Combining ultrasound with NBs helps in drug localization while overcoming off-target effects. NBs utilizing PLGA have garnered attention for targeted drug delivery because of their unique physical and surface properties. PLGA is highly recommended in various medical applications, including sutures, bone implants, and sustained drug release systems, due to its biocompatibility and biodegradability properties.[14] The quadratic model suggested by the design was applied to PS, PdI, ZP, and % EE. Positive coefficients in the model indicated that an increase in associated variables led to higher drug

Table 3. Stability data of the NBs stored at various temperatures

Temperature	Months	PS (nm)	PdI	% EE
5±3 °C	Initial	186.90±13.9	0.146±0.042	66.12±1.48
	0.5	187.82±8.25	0.146±0.057	66.0±1.65
	1	188.38±9.10	0.148±0.044	65.09±3.92
	2	190.48±7.04	0.172±0.034	64.86±3.30
	3	191.26±8.34	0.164±0.037	63.19±3.66
25±2 °C	Initial	186.91±13.9	0.146±0.042	66.12±1.48
	0.5	187.26±2.16	0.149±0.066	66.06±2.85
	1	188.40±2.28	0.154±0.010	64.83±4.60
	2	192.68±4.98	0.180±0.041	63.37±2.89
	3	194.33±5.48	0.246±0.064	62.01±3.58
40±2 °C	Initial	186.89±13.9	0.146±0.042	66.12±1.48
	0.5	189.35±5.26	0.149±0.088	64.58±2.81
	1	194.13±6.06	0.218±0.032	62.22±2.16
	2	196.47±8.70	0.266±0.038	61.79±3.38
	3	199.26±9.52	0.296±0.046	60.10±3.60

PS: Particle size, PdI: Polydispersity index, EE: Encapsulation efficiency, NBs: Nanobubbles

Table 4. Pharmacokinetic parameters

Pharmacokinetic parameters	Pure drug	Drug-loaded NBs	Reference (Marketed)
C_{max} (ng/mL)	93.2±8.14	158.06±8.62	112.89±6.60
T_{max} (h)	6	6	0.5
Half-life (h)	47.70±6.16	52.81±8.40	26.05±6.63
AUC_{0-t} (ng. h/mL)	4382.38±174.28	7178.37±319.94	1380.40±89.94
Ke (h-1)	0.0145	0.0131	0.0266
MRT (h)	68.71±6.21	77.35±7.43	32.60±6.14

NBs: Nanobubbles, AUC: Area under the curve, MRT: Mean residence time

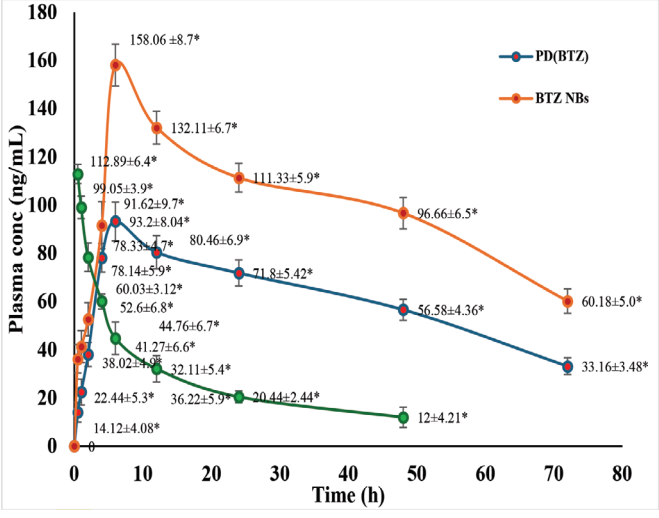

Figure 8. *In vivo* pharmacokinetic studies

entrapment. The concentration of the stabilizer has influenced PS, PdI, and ZP. However, when it came to % EE, a high stabilizer concentration led to a decrease in drug entrapment. PVA, as a stabilizer, has the potential to impede drug entrapment in NBs due to its competition for surface adsorption and the subsequent increase in solution viscosity. Moreover, PVA may hinder drug diffusion into NBs during the formation process. Furthermore, its destabilizing effects can result in premature rupture or aggregation, ultimately diminishing the efficiency of drug entrapment.[31] FTIR studies confirmed compatibility between the drug and excipients. DSC and XRD studies revealed no distinct drug peak in the formulation, indicating the absence of crystalline drug material.[10,28]

Electron microscopy helped in the direct visualization of NBs, assessment of their integrity, and analysis of their gas composition. SEM analysis displayed homogeneous, smooth, spherical NBs. Drug release occurred due to cavitation collapse induced by acoustic waves, disrupting NB structures and

enabling rapid delivery of medication. Ultrasound stability studies indicated the transformation of the gas core from nanodroplets to bubbles, known as acoustic droplet generation.[32] The study aligned with the previous findings on NB stability under varying temperature conditions. The temperature-dependent behaviour observed in PS, ZP, and entrapment emphasizes understanding NB characteristics in diverse environmental conditions for practical drug delivery applications. Different polymer materials submerged in NB dispersions exhibited varied effects on NB number concentrations due to hydrophobic interactions. *In vivo* studies in Wistar rats revealed gradual drug release from the formulation, leading to an increased half-life of the drug with high AUC. These findings indicated a significant improvement in the oral bioavailability of the chosen medicine when using NBs compared to the free drug.[32] The improved bioavailability of NBs with PLGA is achieved through various mechanisms. These include better drug encapsulation within PLGA nanoparticles, longer circulation time due to the protective coating of PLGA, and increased uptake by target cells or tissue. As a result, these mechanisms contribute to enhanced therapeutic outcomes. By enhancing tumor penetration and drug release, US-driven cavitation helps to precisely and site-specifically activate drugs. By combining ultrasound with NBs, drug localization can be achieved while mitigating off-target side effects.Optimizing stability, dose, and safety remains difficult, even if it could help reduce side effects and counteract medication resistance. Clinical acceptance depends on standardizing US characteristics among different modalities. Rigorous trials, translational research, and regulatory validation collectively define the successful incorporation of treatments. To guarantee scalability, large-scale manufacturing has to be cost-effective and efficient. Promoting this technology requires a multidisciplinary strategy to link actual uses with experimental results.

CONCLUSION

This research introduced an innovative approach to improving the solubility of BTZ NBs. By conducting a thorough investigation, the study demonstrated that NBs significantly enhanced the release of the drug, indicating their potential as a new and smart delivery system. Response surface methodology ensured a precise control over the size distribution, resulting in improved uniformity. Additionally, drug-loaded NBs exhibited exceptional stability and dissolvability in the gastrointestinal tract compared to the traditional drug suspensions, suggesting a longer drug half-life and increased effectiveness. These findings highlighted a promising role of PLGA NBs in ultrasound-responsive formulations for cancer therapy, offering notable benefits such as faster dissolution rates, sustained, targeted drug release, and improved oral bioavailability.

Ethics

Ethics Committee Approval: The animal protocol was designed and approved by the Institutional Animal Ethics Committee of Teegala Ram Reddy College of Pharmacy (approval number: 1447/PO/Re/S/11/CPCSEA-97/A, dated: 17.02.2024).

Informed Consent: Not required.

Footnotes

Authorship Contributions

Concept: N.K., K.K.Y., Design: N.K., K.M., K.K.Y., Data Collection or Processing: N.K., Analysis or Interpretation: N.K., Literature Search: N.K., K.M., Writing: N.K., K.M.

Conflict of Interest: The authors declare no conflicts of interest.

Financial Disclosure: The authors declared that this study received no financial support.

REFERENCES

1. Hideshima T, Mitsiades C, Tonon G, Richardson PG, Anderson KC. Understanding multiple myeloma pathogenesis in the bone marrow to identify new therapeutic targets. Nat Rev Cancer. 2007;7:585-598.
2. Wang J, Lv C, Zhou M, Xu JY, Chen B, Wan Y. Second primary malignancy risk in multiple myeloma from 1975 to 2018. Cancers (Basel). 2022;14:4919.
3. Jones CI, Zabolotskaya MV, King AJ, Stewart HJ, Horne GA, Chevassut TJ, Newbury SF. Identification of circulating microRNAs as diagnostic biomarkers for use in multiple myeloma. Br J Cancer. 2012;107:1987-1996.
4. Manasanch EE, Orlowski RZ. Proteasome inhibitors in cancer therapy. Nat Rev Clin Oncol. 2017;14:417-433.
5. Chen D, Frezza M, Schmitt S, Kanwar J, Dou QP. Bortezomib as the first proteasome inhibitor anticancer drug: current status and future perspectives. Curr Cancer Drug Targets. 2011;11:239-253.
6. Lü S, Wang J. The resistance mechanisms of proteasome inhibitor bortezomib. Biomark Res. 2013;1.
7. McConnaughey M. Physical and chemical properties of fungi. In: XPharm: The comprehensive pharmacology reference; 2007:1-3.
8. Mateos MV, San Miguel JF. Safety and efficacy of subcutaneous formulation of bortezomib versus the conventional intravenous formulation in multiple myeloma. Ther Adv Hematol. 2012;3:117-124.
9. Shen S, Du XJ, Liu J, Sun R, Zhu YH, Wang J. Delivery of bortezomib with nanoparticles for basal-like triple-negative breast cancer therapy. J Control Release. 2015;208:14-24.
10. Hong EP, Kim JY, Kim SH, Hwang KM, Park CW, Lee HJ, Kim DW, Weon KY, Jeong SY, Park ES. Formulation and evaluation of a self-microemulsifying drug delivery system containing bortezomib. Chem Pharm Bull (Tokyo). 2016;64:1108-1117.
11. Deshantri AK, Metselaar JM, Zagkou S, Storm G, Mandhane SN, Fens MHAM, Schiffelers RM. Development and characterization of a liposomal formulation of bortezomib. Int J Pharm X. 2019;1:100011.
12. Pitt WG, Husseini GA, Staples BJ. Ultrasonic drug delivery-a general review. Expert Opin Drug Deliv. 2004;1:37-56.
13. Jin J, Yang L, Chen F, Gu N. Drug delivery system based on nanobubbles. Interdiscip Mater. 2022;1:471-494.
14. Makadia HK, Siegel SJ. Poly Lactic-co-glycolic acid (PLGA) as biodegradable controlled drug delivery carrier. Polymers (Basel). 2011;3:1377-1397.
15. Rocha CV, Gonçalves V, da Silva MC, Bañobre-López M, Gallo J. PLGA-based composites for various biomedical applications. Int J Mol Sci. 2022;23:2034.

16. Gao J, Liu J, Meng Z, Li Y, Hong Y, Wang L, He L, Hu B, Zheng Y, Li T, Cui D, Shen E. Ultrasound-assisted *C3F8*-filled PLGA nanobubbles for enhanced *FGF21* delivery and improved prophylactic treatment of diabetic cardiomyopathy. Acta Biomater. 2021;130:395-408.
17. Ponnaganti M, Kishore Babu A. Preparation, characterization and evaluation of chitosan nanobubbles for the targeted delivery of ibrutinib. Vol 8.; 2021. Accessed April 9, 2024. https://www.nveo.org/index.php/journal/article/view/4379
18. Bessone F, Argenziano M, Grillo G, Ferrara B, Pizzimenti S, Barrera G, Cravotto G, Guiot C, Stura I, Cavalli R, Dianzani C. Low-dose curcuminoid-loaded in dextran nanobubbles can prevent metastatic spreading in prostate cancer cells. Nanotechnology. 2019;30:214004.
19. Sampathi S, Amancha R, Dodoala S, Kuchana V. Biodegradable polymeric nanocarriers for oral delivery of antiretroviral drug: pharmacokinetic and *in vitro* permeability studies. J Appl Pharm Sci. 2021;11:28-39.
20. Coulibaly FS, Alnafisah AS, Oyler NA, Youan BC. Direct and real-time quantification of bortezomib release from alginate microparticles using boron (^{11}B) nuclear magnetic resonance spectroscopy. Mol Pharm. 2019;16:967-977.
21. Lopalco A, Iacobazzi RM, Denora N, Stella VJ. Bortezomib aqueous solubility in the presence and absence of D-mannitol: a clarification with formulation implications. J Pharm Sci. 2021;110:543-547.
22. Hernandez C, Abenojar EC, Hadley J, de Leon AC, Coyne R, Perera R, Gopalakrishnan R, Basilion JP, Kolios MC, Exner AA. Sink or float? Characterization of shell-stabilized bulk nanobubbles using a resonant mass measurement technique. Nanoscale. 2019;11:851-855.
23. Su C, Ren X, Nie F, Li T, Lv W, Li H, Zhang Y. Current advances in ultrasound-combined nanobubbles for cancer-targeted therapy: a review of the current status and future perspectives. RSC Adv. 2021;11:12915-12928.
24. Burgess MT, Porter TM. Control of acoustic cavitation for efficient sonoporation with phase-shift nanoemulsions. Ultrasound Med Biol. 2019;45:846-858.
25. Kyzas GZ, Mitropoulos AC. From bubbles to nanobubbles. Nanomaterials (Basel). 2021;11:2592.
26. Xu JS, Huang J, Qin R, Hinkle GH, Povoski SP, Martin EW, Xu RX. Synthesizing and binding dual-mode poly (lactic-co-glycolic acid) (PLGA) nanobubbles for cancer targeting and imaging. Biomaterials. 2010;31:1716-1722.
27. Danaei M, Dehghankhold M, Ataei S, Hasanzadeh Davarani F, Javanmard R, Dokhani A, Khorasani S, Mozafari MR. Impact of particle size and polydispersity index on the clinical applications of lipidic nanocarrier systems. Pharmaceutics. 2018;10:57.
28. Mahmoudian M, Valizadeh H, Zakeri-Milani P. Bortezomib-loaded solid lipid nanoparticles: preparation, characterization, and intestinal permeability investigation. Drug Dev Ind Pharm. 2018;44:1598-1605.
29. Marinaro WA, Schieber LJ, Munson EJ, Day VW, Stella VJ. Properties of a model aryl boronic acid and its boroxine. J Pharm Sci. 2012;101:3190-3198.
30. Foudas AW, Kosheleva RI, Favvas EP, Kostoglou M, Mitropoulos AC, Kyzas GZ. Fundamentals and applications of nanobubbles: a review. Chem Eng Res Des. 2023;189:64-86.
31. Wiśniewska M, Ostolska I, Szewczuk-Karpisz K, Chibowski S, Terpiłowski K, Gun'ko VM, Zarko VI. Investigation of the polyvinyl alcohol stabilization mechanism and adsorption properties on the surface of ternary mixed nanooxide AST 50 (Al_2O_3-SiO_2-TiO_2). J Nanopart Res. 2015;17:12.
32. Rani S, Sahoo RK, Nakhate KT, Ajazuddin, Gupta U. Biotinylated HPMA centered polymeric nanoparticles for bortezomib delivery. Int J Pharm. 2020;579:119173.

Supplementary Table 1. Physicochemical and pharmacokinetic properties of bortezomib

Molecular structure	
IUPAC name	[(1R)-3-methyl-1-[[(2S)-3-phenyl-2-(pyrazine-2-carbonylamino) propanoyl] amino]butyl]boronic acid
Molecular weight	384.243
logP	0.89 (ALOGPS)
logP	1.53 (ChemAxon)
pKa (strongest acidic)	13.04 (ChemAxon)
pKa (strongest basic)	–0.7 (ChemAxon)
Water solubility	0.0532 mg/mL
Physiological charge	0

IUPAC: International Union of Pure and Applied Chemistry

Supplementary Table 2. FTIR spectral data with wave number and the corresponding groups

Wave number (cm^{-1})	Corresponding group in pure drug	Wave number (cm-1)	Corresponding group in pure drug
3446.9	O-H stretching, typical in alcohols and phenols	1394	B-O stretching
3294.18	O-H stretching in B-O-H group of BTZ	1261.49	C-N stretching, potentially from amines or amides.
2937.68	C-H stretching, suggesting alkanes or methyl groups.	1193.98	C-O stretching (ethers or esters)
1747.57	C=O stretching of carbonyl groups (ketones or aldehydes)	1085.96	C-O stretching (alcohols, ethers, or esters).
1663	C=C stretching, typical of alkenes or aromatic compounds	1022	C-N stretching (amines or amides)
1523.9	amide C=O stretching	885.36	C-H bending (alkanes or methyl groups)
1460	C-H bending (alkanes or methyl groups)	719.47	C-H bending (alkanes or methyl groups)

BTZ: Bortezomib, FTIR: Fourier transform infrared spectroscopy

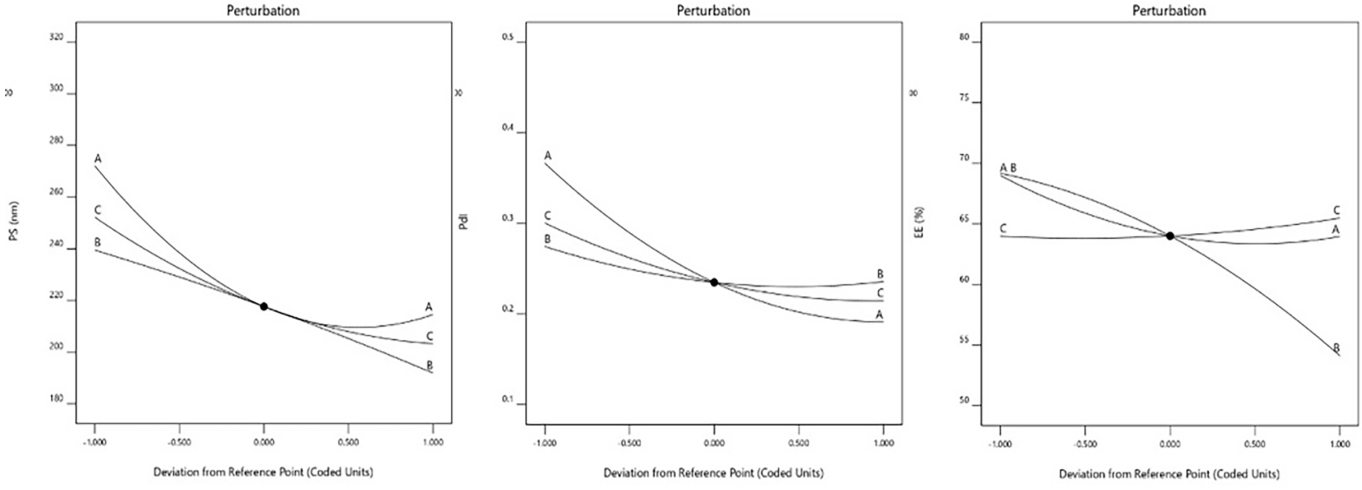

Supplementary Figure 1. Perturbation plots of PS, Pdl, and EE

PS: Particle size, Pdl: Polydispersity index, EE: Encapsulation efficiency

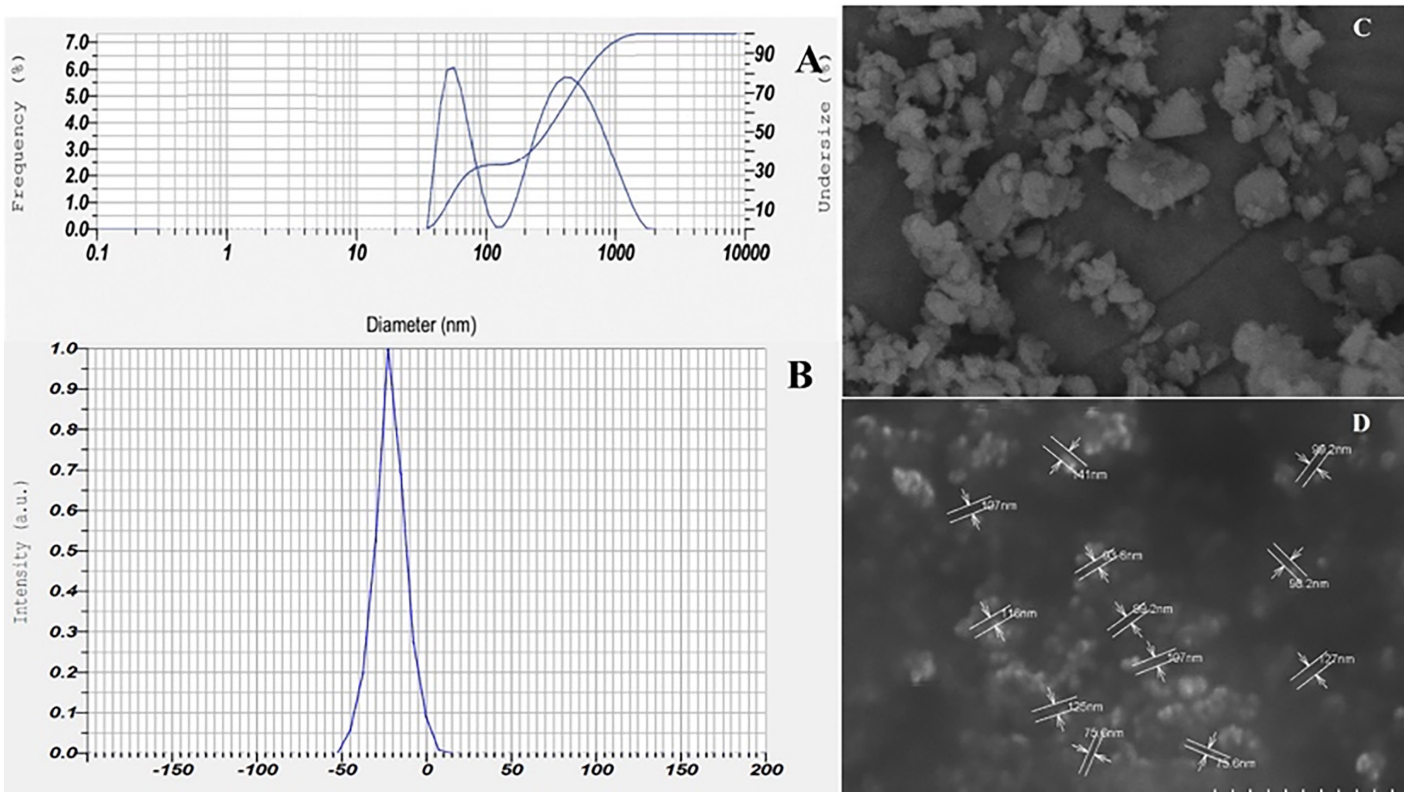

Supplementary Figure 2. A) Particle size; B) ZP; C) SEM of plain drug; D) SEM of optimized NBs
EE: Encapsulation efficiency, ZP: Zeta potential, SEM: Scanning electron microscopy

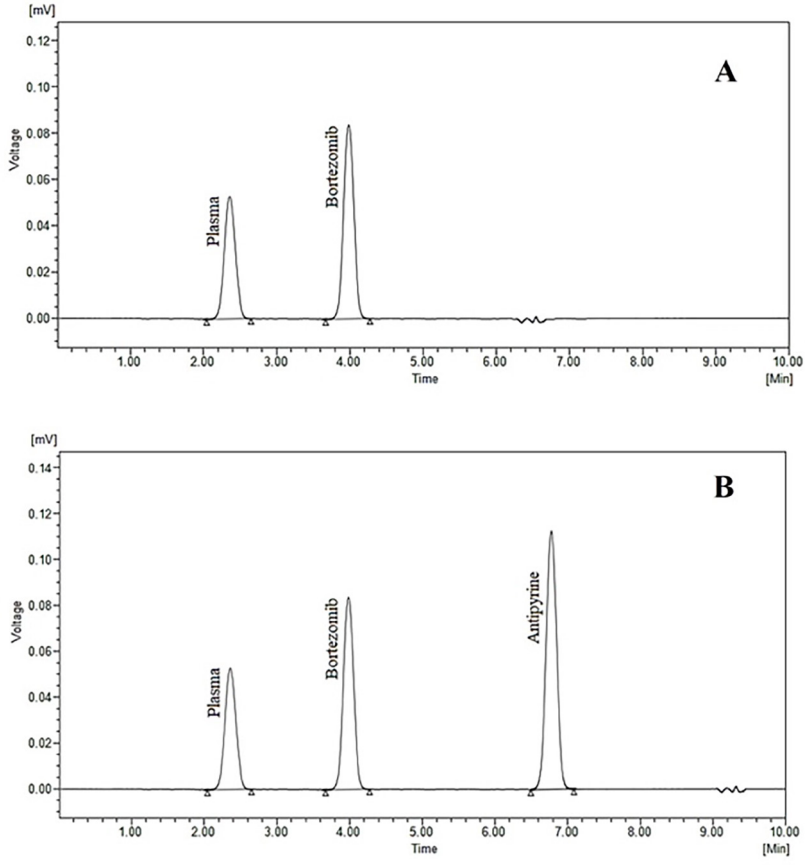

Supplementary Figure 3. Bioanalytical method development of the drug in plasma (A), and drug and internal standard in plasma (B)